

Received: 2016.12.23  
Accepted: 2017.03.01  
Published: 2017.09.03

# Quantitative Visualization of Dynamic Tracer Transportation in the Extracellular Space of Deep Brain Regions Using Tracer-Based Magnetic Resonance Imaging

Authors' Contribution:  
Study Design A  
Data Collection B  
Statistical Analysis C  
Data Interpretation D  
Manuscript Preparation E  
Literature Search F  
Funds Collection G

BCDEF 1 **Jin Hou\***  
CG 2 **Wei Wang\***  
D 3 **Xianyue Quan**  
DF 3 **Wen Liang**  
BC 1 **Zhiming Li**  
AG 2 **Hongbin Han**  
AFG 1 **Deji Chen**

1 Department of Radiology, The 2<sup>nd</sup> Affiliated Hospital of Guangzhou Medical University, Guangzhou, Guangdong, P.R. China  
2 Department of Radiology and Peking Magnetic Resonance Imaging Technology Research Laboratory, 3<sup>rd</sup> Hospital of Peking University, Beijing, P.R. China.  
3 Department of Radiology, Zhujiang Hospital, Southern Medical University, Guangzhou, Guangdong, P.R. China

\* Jin Hou and Wei Wang are co-first authors

**Corresponding Authors:**

Deji Chen, e-mail: [chendeji2003@163.com](mailto:chendeji2003@163.com), Hongbin Han, e-mail: [651464635@qq.com](mailto:651464635@qq.com)

**Source of support:**

This project was funded by the National Natural Science Foundation of China (No.81471633), the Beijing Municipal Science and Technology Commission (No. Z161100000116041), the China Postdoctoral Science Foundation Grant (No. 2015M570901), and the Medical and Health Technology Project in Guangzhou (No. 20141A011008, 20151A011075), the National Science Fund for Distinguished Young Scholars (No.61625102)

**Background:** This study assessed an innovative tracer-based magnetic resonance imaging (MRI) system to visualize the dynamic transportation of tracers in regions of deep brain extracellular space (ECS) and to measure transportation ability and ECS structure.





**Material/Methods:** Gadolinium-diethylene triamine pentaacetic acid (Gd-DTPA) was the chosen tracer and was injected into the caudate nucleus and thalamus. Real-time dynamic transportation of Gd-DTPA in ECS was observed and the results were verified by laser scanning confocal microscopy. Using Transwell assay across the blood-brain barrier, a modified diffusion equation was further simplified. Effective diffusion coefficient  $D^*$  and tortuosity  $\lambda$  were calculated. Immunohistochemical staining and Western blot analysis were used to investigate the extracellular matrix contributing to ECS structure.

**Results:** Tracers injected into the caudate nucleus were transported to the ipsilateral frontal and temporal cortices away from the injection points, while both of them injected into the thalamus were only distributed on site. Although the caudate nucleus was closely adjacent to the thalamus, tracer transportation between partitions was not observed. In addition,  $D^*$  and the  $\lambda$  showed statistically significant differences between partitions. ECS was shown to be a physiologically partitioned system, and its division is characterized by the unique distribution territory and transportation ability of substances located in it. Versican and Tenascin R are possible contributors to the tortuosity of ECS.

**Conclusions:** Tracer-based MRI will improve our understanding of the brain microenvironment, improve the techniques for local delivery of drugs, and highlight brain tissue engineering fields in the future.

**MeSH Keywords:** **Brain • Diffusion • Extracellular Space • Magnetic Resonance Imaging**

**Full-text PDF:** <https://www.medscimonit.com/abstract/index/idArt/903010>

 4103  —  4  41



## Background

Brain tissue is anatomically composed of 3 compartments: neural cells, vascular system, and brain extracellular space (ECS). Although neural cells have long been considered as the most important functional element of the brain, they only occupy 70–80% of the total brain volume [1,2]. The vascular system and ECS together form the brain microenvironment (BME), which takes up the rest of the brain volume and provides a living environment for neural cells. The ECS occupies 15–20% of the total brain volume and is an irregular, tortuous, and narrow space between the capillaries and neural cells, and between adjacent neural cells. The width of the ECS between cell bodies mostly ranges from 38 to 64 nanometers and the space is about 20 nanometers between synapses [3]. The ECS contains interstitial fluid and various molecules [4], and plays a number of active and positive roles in brain functions, including cell-to-cell communication, information processing and integration, and coordinated responses to changes in the external and internal environment of the brain [5,6]. Compared with the investigations into the other 2 compartments, the techniques used to investigate the ECS are poor due to the narrow space. Most current knowledge on ECS *in vivo* is derived from research by Nicholson et al., who provided real-time iontophoresis (RTI) and integrative optical imaging techniques (IOI) [1]. Using advanced equipment, the structure (size and geometry) of the ECS *in vivo* can be determined, especially for ECS parameters around 200  $\mu\text{m}$  in depth or width. However, the advanced techniques require ingenious design and have limited detection range. Based on their outstanding work, we propose a novel tracer-based magnetic resonance imaging (MRI) system to evaluate the nanoscale ECS structure. The ECS can be considered to have an elastic porous structure, and a diffusion equation can be applied for remodeling the transportation of substances in the ECS.

Using reasonable approximations and appropriate experimental protocols, the diffusion equation can be further simplified and the parameters (tortuosity and effective diffusion coefficient) can be calculated.

MRI has been widely used for *in vivo* imaging of biological tissues and investigating brain anatomy at submillimeter level, because of its advantages such as non-ionization damage, excellent soft-tissue contrast, real-time monitoring, and multi-view imaging [7,8]. Gadolinium-diethylene triamine pentaacetic acid (Gd-DTPA) is frequently used as a positive contrast agent in clinical applications to reduce the T1 time of water protons from an effective distance of 2.5 angstroms, and to increase signal intensity on MR images [9]. It has been used to simulate or trace substance transportation in brain ECS in previous studies [10,11]. Compared with other ions or fluorescence-labeled tracers, Gd-DTPA has many advantages, including biomedical

inertness, thermal stability, and small molecular weight (938 Da), and it rarely translates into nerve cells [12–14]. Moreover, Gd-DTPA at this concentration does not cause any distortion or artifacts of brain parenchyma on MRI. These advantages make Gd-DTPA well-suited for the measurement and imaging of brain ECS. Most importantly, a prior study indicated that the concentration of Gd-DTPA on MR images can be calculated in real time with the net increase of MRI signal [15]. Therefore, the MRI tracer-based method not only globally visualizes the dynamic transportation of tracers in the ECS of deep brain regions (caudate nucleus and thalamus), but also quantifies their characteristics in tracer transportation (effective diffusion coefficients) and ECS structure (tortuosity).

The tortuosity of the ECS can be determined by boundary structures containing cell membrane and extracellular matrix (ECM) [16]. ECM is a highly hydrated mesh-like structure that mainly consists of several families in the brain, including glycosaminoglycans, proteoglycans, glycoproteins (tenascin, reelin, laminin, and fibronectin), and fibrous proteins [17–19]. The mesh-like structure of ECM can interfere with the brain interstitial fluid (ISF) flow or substance transportation in the ECS. The side-chains of ECM floating inside ISF may further increase the friction and resist substance transportation in the ECS [20]. Moreover, negatively charged components in ECM may disturb the movement of charged substances in the ECS. In the present study, we investigated the ECS by MR method, using Gd-DTPA as a tracer. Modified diffusion equation and imaging post-processing techniques were also used. Using immunohistochemistry and Western blotting, we investigated the expression of a spectrum of ECM molecules, including Tenascin C (TNC), Tenascin R (TNR), and Versican, to explain the difference in tortuosity between the caudate nucleus and thalamus.

## Material and Methods

### Reasonable approximations of diffusion equation

To describe the transportation of substances in ECS, Nicholson et al. provided a modified diffusion Eq (1) [21].

$$\frac{\partial C}{\partial t} = (D/\lambda^2) \cdot \nabla^2 C + Q/\alpha - v \cdot \nabla C - f(C)/\alpha \quad (1)$$

Here,  $C$  (mM) represents the amount of substance concentration in the ECS, and it is a result of position and time ( $t$ ) (s). The  $\partial C/\partial t$  represents the changes in concentration per time at a particular position.  $D$  ( $\text{cm}^2/\text{s}$ ) represents the free diffusion coefficient.  $\lambda$  represents the characteristics of limitation towards diffusion observed within the ECS in contrast to that in free solution. Because the brain tissue structure causes anisotropic diffusion,  $\lambda$  has become a tensor rather than a scalar.  $D/\lambda^2 = D^*$  is the effective diffusion coefficient. The symbols  $\nabla^2$

and  $\nabla$  indicate the first-order and second-order derivatives in the appropriate coordinate system.  $Q$  (mM/s) is the source term.  $\alpha$  represents volume fraction.  $v$  represents the velocity of bulk flow. The last expression,  $f(C)$  ( $s^{-1}$ ), stands for the clearance or removal of substances from the ECS directly into the cells, located transversely from the blood brain barrier (BBB), or by enzyme degradation. A direct linear relationship between the increment in signal intensity  $\Delta SI$  and  $C$  was observed in a previous study [15]. The term  $Q/\alpha$  reflects the fact that Gd-DTPA injected into the brain is restricted in the ECS rather than diffusing to the entire brain.  $Q$  is determined by the releasing method of Gd-DTPA into the ECS. In the present study, a total quantity of 2  $\mu$ L solution of Gd-DTPA (10 mM) was automatically inoculated at a proportion of 0.2  $\mu$ L per min during a 10-min period. Typical value  $\alpha$  is 20%.  $v$  (cm/s) can be neglected according to a previous study, if it involves temporary and close-distance diffusion happening all over the ECS medium rather than the perivascular space [22]. Above all, if an ideal brain model with known  $\alpha$  can be developed,  $Q$  can be controlled, in addition of  $f(C)=0$  can be verified, diffusion Eq (2) can be applied to calculate nanostructure parameters  $\lambda$  and  $D^*$ , in which  $\partial C/\partial t$  can be measured by the changes in signal enhancement ( $\Delta SI$ ).

$$\partial C/\partial t = (D/\lambda^2) \cdot \nabla^2 C + Q/\alpha \quad (2)$$

### Transwell assay

The establishment and assessment methods for BBB were derived from that described by Xie et al. [23]. To establish an *in vitro* model of BBB, microvascular endothelial cells (BMVEC) were isolated from the cerebral cortex of BALB/c mice (Department of Laboratory Animal Science, Peking University, China) and purified using density centrifugation. Cells were re-suspended in Dulbecco's modified Eagle's medium holding a solution of 20% fetal calf serum, 100 mg/L streptomycin, 100 000 U/L penicillin, 100 mg/L endothelial cell growth factor, 2 mM L-glutamine, 40 mU/L insulin, and 20 mg/L heparin. Then, the cells were seeded into 1% gelatin-coated culture flasks and fed every 2 days with fresh medium until the cells became a confluent monolayer. BMVEC were seeded on the bottom side of the gelatin-coated 24-well Transwell inserts (Corning Lim Sciences, MA) at the density of 200 000 cells/cm<sup>2</sup>. In a 37°C and 5% CO<sub>2</sub> humidified incubator, BBB models were established within 3 days. The integrity of BBB was judged by a 4-h water-leaking test. Culture medium was added into the apical chamber to make the liquid level in the apical chamber higher than that in the basolateral chamber (>0.5 cm). If the fluid level was maintained (>0.4 cm) after incubation for 4 h, we considered that the BBB had been established. Based on the establishment of BBB *in vitro*, the standard sample containing Gd-DTPA was diluted into different concentrations (0.1, 1, and 10 mM) using 5% serum and phenol red-free medium. The 460-mL dilution

was added into the apical chamber and 1140  $\mu$ L was added into the basolateral chamber to maintain the same level of liquid surface in the Transwell inserts. The Transwell inserts were placed into the incubator. Then, 50  $\mu$ L medium was transferred from the basolateral chamber for measuring the concentrations using Inductively Coupled Plasma Mass Spectrometry at time points of 0, 1, 2, 4, 6, 9, and 11 h. The permeation rate of Gd-DTPA was derived from the concentration-time curve. The permeation rate of peroxidase crossing the BBB was also measured for the control group.

### MR scanning

MR scanning was performed on a 3.0 Tesla MRI scanner (Magnetom Trio; Siemens Healthcare, Erlangen, Germany) The 8-channel wrist array coil and T<sub>1</sub> three-dimensional magnetization-prepared rapid gradient echo (3DMP-RAGE) sequence were used. Scanning parameters included: repetition time 1500 ms, echo time 3.7 ms, inversion time 900 ms, flip angle 12°, field of view 267 mm, spatial resolution 0.5×0.5×0.5 mm<sup>3</sup>, and scanning time 290 s. Using artificial cerebrospinal fluid, 10 mM Gd-DTPA was produced as the tracer by dilution.

MR images of the same subject were processed before and after the injection, as described in detail previously [24,25]. Briefly, a MATLAB-based analysis software was developed independently. With the aid of this software, all images were co-registered using similarity detection, rigid transformation, and adaptive stochastic gradient descent algorithm. These pre-injection images were then subtracted from the post-injection images. The acquired "bright pixels" in the post-processed images were considered as the areas where the tracer was present. The signal intensity of bright pixels was represented as  $\Delta SI$ . In the agarose experiment, we propose the weighted  $\Delta SI$  ( $\Delta SI$  multiplied by bright pixels) as the term predicting the amount of Gd-DTPA. We propose  $\Delta SI$  as the  $C$ , which were the key points to calculate the parameters of ECS. The time during which  $\Delta SI$  was decreased to zero was evaluated.

### Agarose experiment

Agarose gel was produced through dissolving 0.3 g agarose powder in 100 mL of 0.9% brine medium. The agarose gels were kept at 37±0.5°C and pre-injection MRI was performed. We infused 2  $\mu$ L 10 mM Gd-DTPA solution into agarose gel at the speed of 0.2  $\mu$ L/min and 0.4  $\mu$ L/min, respectively, using a 10  $\mu$ L microsyringe (Hamilton, Bonaduz AG, Switzerland) and auto-infusing device (Harvard Apparatus, Holliston, MA). A series of MR T<sub>1</sub> 3DMP-RAGE were performed at after-injection time points of 5, 10, 30, 50, 70, and 90 min.

## Animals

Twenty male Sprague-Dawley rats (weight 250–300 g, ages 6–8 weeks) were obtained from the Department of Laboratory Animal Science, Peking University Health Science Center, China. The rats were randomly divided into caudate nucleus-injected sets ( $n=10$ ) and thalamus-injected sets ( $n=10$ ). The rats were anesthetized via an intraperitoneal injection of a mixture of magnesium sulfate, ethanol, pentobarbital sodium, chloral hydrate, and propylene glycol. Its original dose was 3 mL/kg and the maintenance dose was 0.7 mL/kg/h. We maintained body temperature of rats at  $38\pm 0.5^\circ\text{C}$  by use of a heating pad and monitored body temperature using a rectal thermometer. MR scanning and post-processing were done according to the MRI tracer-based method described in detail previously [13]. In brief, the bregma sutures of rats were exposed and pre-injection MR images of brains were acquired. Using the stereotactic coordinate system (Lab Standard Stereotaxic-Single, Stoelting Co., Wood Dale, USA), and auto-infusing device, Gd-DTPA was infused into the target positions. The injection site of the caudate nucleus was 1.0 mm (the anterior–posterior),  $-3.5$  mm (the medial–lateral), and  $-6$  mm (the dorsal–ventral), and that of the thalamus was  $-3.5$  mm (the anterior–posterior),  $-6.5$  mm (the dorsal–ventral), and  $-2.0$  mm (the medial–lateral) [26]. The volume of 2  $\mu\text{L}$  Gd-DTPA was infused into the target positions at the speed of 0.2  $\mu\text{L}/\text{min}$  for a period of 10 min, followed by a 5-min waiting period to reduce the reflux. Multi-period MR scanning was performed to acquire post-injection images and the scanning time was 15, 30, 60, 120, 180, 240, 300, 360, 420, 480, and 540 min. Experiments were approved by the Ethics Committee of Peking University Health Science Center (No. LA2012-016).

## Laser scanning confocal microscopy (LSCM)

To verify findings demonstrated by MRI, *in vitro* fluorescence imaging was performed using LSCM (TCS SP8 MP, Leica, Germany). Lucifer Yellow (LY) (Sigma-Aldrich, St. Louis, MO), the extracellular fluorescent tracer, was injected into the caudate nucleus and thalamus. Before the injection of LY into rat brains, MRI was performed in all rat brains to localize and determine the injection point and route, which also provided a reference for sample slices for LSCM images. The rats were sacrificed and cerebral tissues were freed every 1 h until 6 h after injection. The distribution areas of LY were confirmed using LSCM and compared with results shown in MRI.

## Immunohistochemical analysis

The rats were anesthetized. Before the brains were removed, 4% paraformaldehyde was transcardially perfused and fixed immediately. The tissues were post-fixed overnight at  $4^\circ\text{C}$  and paraffin-inserted and divided up in compliance with standard

procedures. We de-paraffinized 5- $\mu\text{m}$  sections from the caudate nuclei and thalamus, then treated them with hydrogen peroxide (0.3%). Immunohistochemical staining was performed using peroxidase antiperoxidase technique after heat antigen-retrieval procedure. Three rabbit antibodies directed against TNC, TNR, and Versican (all from Abcam, Cambridge, UK) were diluted and incubated on sections overnight at  $4^\circ\text{C}$ . We then used secondary antibody (PV-6001; Zhongshan Goldenbridge Biotechnology Co. Ltd., Beijing, China) to treat the sections for 30 min at  $37^\circ\text{C}$  incubation. Lastly, the slides were stained through and incubated with 3, 3'-diaminobenzidine and hematoxylin and eosin.

## Western blotting

ECM levels in caudate nucleus and thalamus were detected by Western blotting. Briefly, equivalent protein amount (50  $\mu\text{g}$ ) was separated by 12% Tris polyacrylamide gel and transported into polyvinylidene difluoride membrane (Bio-Rad, Hercules, CA), which was then stored for 1 h in TBST containing 5% defatted milk and incubated with antibodies against TNR (R&D Systems, Minneapolis, MN) overnight at  $4^\circ\text{C}$ . Membranes were then incubated together with the secondary antibody. Bound antibodies were visualized by enhanced chemiluminescence.

## Statistical evaluation

All the derived data were evaluated with the Windows version of SPSS 19.0 and are expressed by means  $\pm$ SD. The differences in permeability of Gd-DTPA crossing the BBB and free samples were compared using paired *t* tests. The *t* tests were used to compare effective diffusion coefficient ( $D^*$ ) and tortuosity ( $\lambda$ ) between the caudate nucleus and thalamus. When the *P* value was  $<0.05$ , the disparity was statistically significant.

## Results

### Permeability of Gd-DTPA crossing the BBB *in vitro* is higher than that of POD, and is not affected by concentration

To test the permeability of Gd-DTPA crossing the BBB *in vitro*, Transwell assay was performed. The fluid level was maintained ( $>0.4$  cm) after incubation for 4 h, suggesting that the BBB had been established (Figure 1A–1D). The permeation rate of Gd-DTPA increased linearly with time and the concentrations did not significantly influence permeation rates ( $n=3$ ; paired *t* test,  $t=0.763$  vs.  $0.379$  vs.  $0.848$ ,  $P>0.05$ ). The mean permeation rate of Gd-DTPA was less than  $0.218\pm 0.060\%/h$  in 12 h, which was significantly higher than the mean permeation rate of peroxidase ( $0.120\pm 0.023\%/h$ ) ( $n=3$ ; paired *t* test,  $t=0.020$  vs.  $0.030$  vs.  $0.015$ ,  $P<0.05$ ) (Figure 1E). The derived outcomes indicate that the permeability of Gd-DTPA crossing



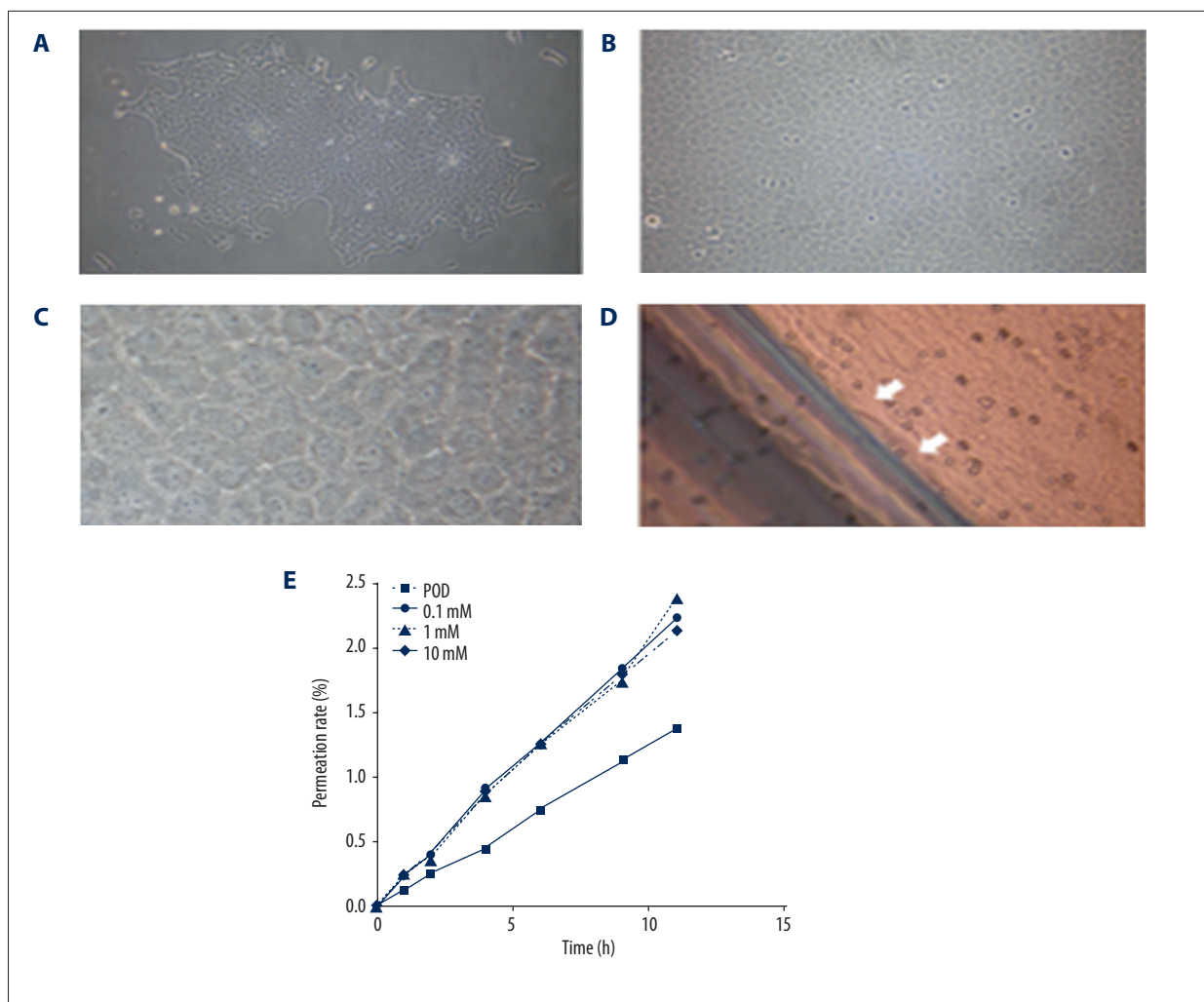


**Figure 1.** Permeability of Gd-DTPA crossing the BBB *in vitro*. Microvascular endothelial cells on (A) day 2 (×40), (B) day 3 (×100), and (C) day 3 (×400). (D) Established membrane adherent to the bound of inserts indicated by white arrows. (E) Permeation rate of 0.1, 1, and 10 mM Gd-DTPA and POD at various time points in the BBB model *in vitro*.

the BBB *in vitro* was higher than that of POD, and was not affected by concentration.

**Weighted  $\Delta SI$  was maintained longer with lower injection rate of Gd-DTPA**

To determine weighed  $\Delta SI$ , an agarose experiment was performed. After Gd-DTPA was injected into agarose at different rates, weighed  $\Delta SI$  was temporarily increased and reached peaks at different time points. In the high injection rate (0.4  $\mu\text{L}/\text{min}$ ) group, weighed  $\Delta SI$  decreased quickly, but in the low injection rate (0.2  $\mu\text{L}/\text{min}$ ) group, weighed  $\Delta SI$  was maintained for 90 min (Figure 2). The results suggest that weighed  $\Delta SI$  was maintained longer with a lower injection rate of Gd-DTPA.

**Transportation of Gd-DTPA and LY in the thalamus was quicker than that in the caudate nucleus**

Gd-DTPA and LY injected into the caudate nucleus were transported to the ipsilateral frontal and temporal cortices away from the injection points, while both of them injected into the thalamus were only distributed on site. Although the caudate nucleus was closely adjacent to the thalamus, Gd-DTPA and LY transportation between them was not observed (Figure 3).

In addition, effective diffusion coefficients ( $D^*$ ) and tortuosity ( $\lambda$ ) of the ECS showed significant differences between the caudate nucleus and thalamus ( $D^*=3.12\pm 1.00\times 10^{-6}\text{ cm}^2/\text{s}$  and  $3.78\pm 0.89\times 10^{-6}\text{ cm}^2/\text{s}$ , respectively;  $\lambda=1.29\pm 0.48$  and  $1.17\pm 0.25$ , respectively;  $P<0.05$ ). The time during which  $\Delta SI$  was decreased to zero was significantly different between the caudate nucleus and thalamus ( $t=308\pm 38$  min and  $228\pm 41$  min,

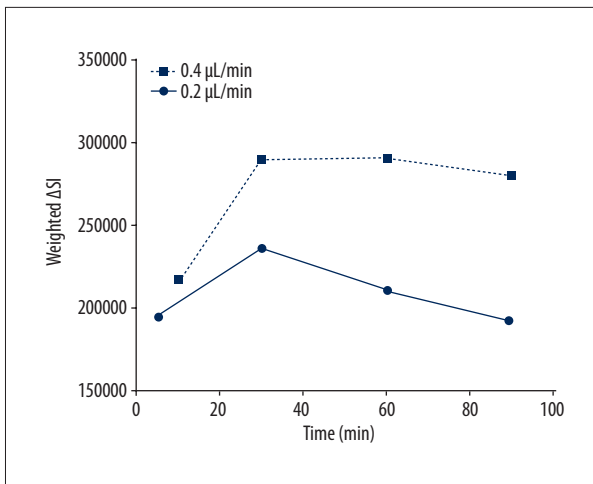


**Figure 2.** Curves of weighted  $\Delta SI$  in agarose. A volume of 2  $\mu\text{L}$  Gd-DTPA solution (10 mM) was automatically injected into the center of gel phantom at different rates (0.2  $\mu\text{L}/\text{min}$  and 0.4  $\mu\text{L}/\text{min}$ ) using a 10- $\mu\text{L}$  microsyringe and auto-infusing device. A series of MR T1 3DMP-RAGE were performed at after-injection time points of 5 min, 10 min, 30 min, 50 min, 70 min, and 90 min.

respectively;  $P < 0.05$ ). The results indicate that transportation of Gd-DTPA and LY in the thalamus was quicker than that in the caudate nucleus.

### TNR and Versican are possible contributors to the tortuosity of ECS

To better explain the difference in tortuosity between the caudate nucleus and thalamus, immunohistochemistry and Western blotting were performed. Minor expression of TNC was observed in both the caudate nucleus and thalamus, but the expression of TNR in both caudate nucleus and thalamus was high, with that of TNR in the thalamus being higher than that in the caudate nucleus according to Western blot analysis. Versican expression was relatively higher in the patch (striosome) compartments of the caudate nucleus, which was related with myelinated fibers (Figure 4). This result suggests that both TNR and Versican are possible contributors to the tortuosity of ECS.

### Discussion

The permeability rate of Gd-DTPA crossing the BBB *in vitro* is less than 0.218%/h and is almost twice as much as that of POD. Because the molecular weight of Gd-DTPA (938Da) is much lower than that of POD (44 kDa), Gd-DTPA can be considered as a substance that does not penetrate the BBB. Gd-DTPA is biomedically inert and is free from enzyme degradation. Furthermore, Gd-DTPA rarely is quickly translated into nerve cells. Therefore, Gd-DTPA is strictly restricted in the ECS and the clearance term  $f(C)$  is approximately zero in Eq. (1).

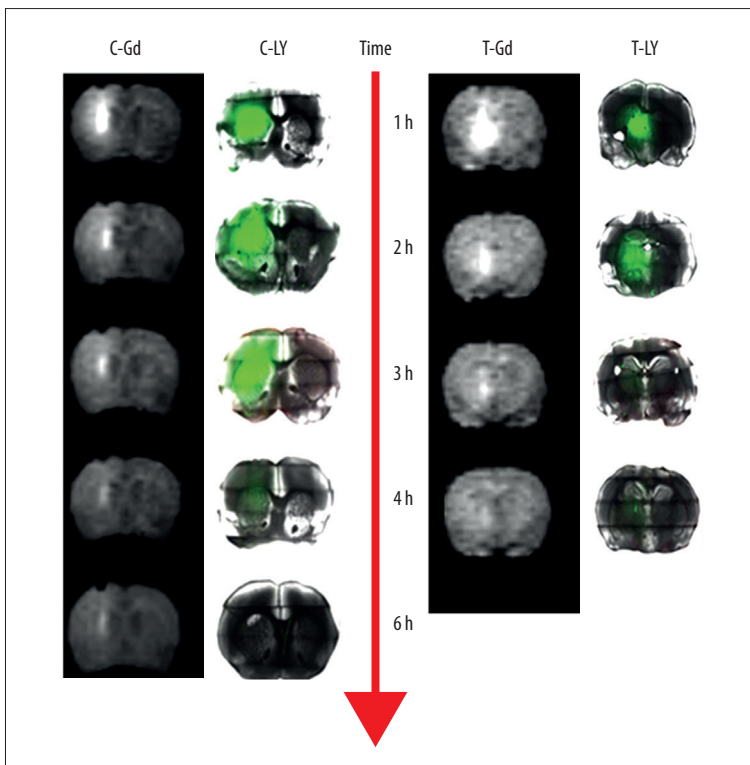


**Figure 3.** Transportation of Gd-DTPA and Lucifer Yellow in rat brain ECS. C-Gd, Gd-DTPA in caudate nucleus; C-LY, Lucifer Yellow in caudate nucleus; T-Gd, Gd-DTPA in thalamus; C-LY, Lucifer Yellow in thalamus.

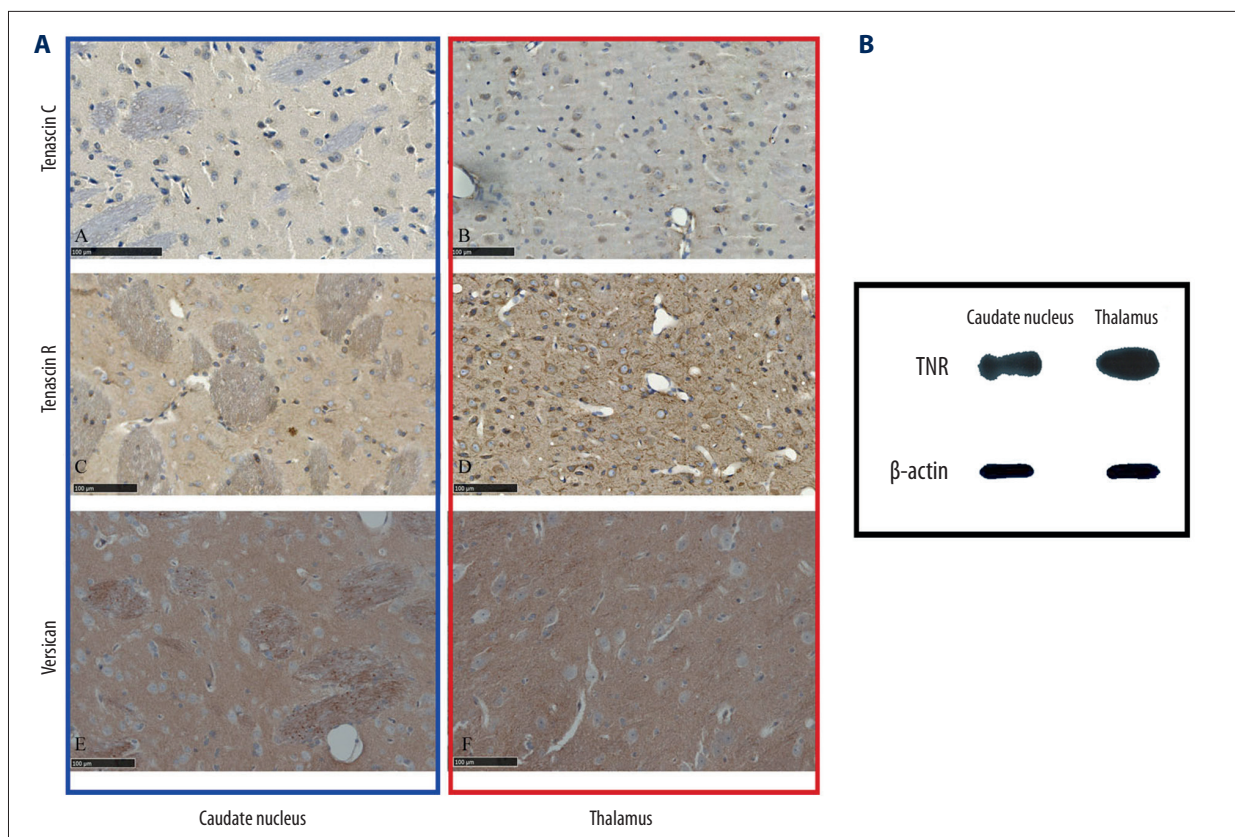


**Figure 4.** Tenascin C (TNC), Tenascin R (TNR), and Versican expression in caudate nucleus and thalamus. **(A)** Representative sections of TNC, TNR, and Versican stained using immunohistochemistry in paraffin sections of caudate nucleus and thalamus. Scale bar=100 µm. **(B)** Representative Western blots of TNR in caudate nucleus and thalamus.

The signal intensity of MR can be influenced by many factors, such as radio frequency pulse, magnetic field strength, and relaxation time. The increment in signal intensity ( $\Delta SI$ ), which can be calculated using self-developing software, is used as the quantitative basic data. In a prior study, a direct linear relationship between  $\Delta SI$  and  $C$  was observed over the concentration range of 0-1 mM [15]. In the agarose experiment, weighted  $\Delta SI$  predicted the amount of Gd-DTPA. Therefore, it is reasonable that the concentration of Gd-DTPA in ECS is transformed to  $\Delta SI$ . Through reasonable approximations and variable transformation, Eq. (1) can be reasonably approximated to Eq. (2), and effective diffusion coefficient and tortuosity can be calculated.

To date, there are 3 approaches developed to investigate the ECS *in vivo*: RTI, IOI, and tracer-based MRI. RTI can calculate the parameters of the ECS within the distance range of approximately 100–200 µm, but it cannot provide the images. IOI can both measure the parameters of ECS and image the transport of tracer in ECS. However, IOI cannot investigate the ECS deeper than 200 µm due to excessive light scattering. Using the tracer-based MRI technique, we have directly visualized tracer transportation in global brain ECS in real time. It has been believed

that the brain ECS is highly connected at any given point, and molecules like water can travel through multiple pathways to reach nearby locations. Nonetheless, our result does not support this hypothesis, and no random distribution of the tracer was shown from the thalamus and caudate nucleus. Gd-DTPA in the caudate has presented eccentric ellipse diffusion, with its main axis being towards the ipsilateral frontotemporal cortex. Little tracer was diffused into the nearby thalamus region. Gd-DTPA in the thalamus was diffused from the injection point and localized mainly within its anatomical division, with no distribution being found in the nearby caudate nucleus. There seems to be a barrier that hinders the cross-regional transportation between the caudate nucleus and thalamus. Moreover, the ability and rate of tracer transportation in the ECS of the 2 regions were different. Therefore, substance transportation in the ECS is sophisticated, presenting divisional characteristics. Transportation in the ECS is important in maintaining physiological functions. For example, neurotransmitters are more quickly and effectively transported to target regions by the ECS rather than by blood circulation through the wall of capillaries [27]. Moreover, the investigation of transportation characteristics of drugs in the ECS is helpful for the development of effective techniques for brain therapeutics; for

example, convection-enhanced delivery where the drug is directly delivered into the ECS to exert neuro-protective or anti-cancer functions bypassing the BBB [28–30]. Theoretically, the delivery technique offers more advantages over conventional drug delivery methods, including less severe adverse effects and higher effectiveness. More recently, the administration of small-dose cytidine diphosphate choline using this technique has been proven to be more efficient in preventing brain ischemia than conventional methods [31].

There are several factors that can influence the transportation, including ECM, artery pulsing, and molecular and ISF properties (velocity, temperature, and viscosity). Because the ECS is enveloped by ECM, ECM can also influence tortuosity. Moreover, the components of ECM may interfere with water molecule or substances, influencing their movements [20]. The present study demonstrated that the expression of TNC was absent from the caudate nucleus and thalamus of mature brains and is present at low levels in the subventricular zone. Our results are consistent with a study reporting that the expression patterns of TNC in the central nervous system depend on the developmental stage and the specific locations [32]. In the developing brain, TNC is expressed on embryonic day 10 and is prominently expressed by neural crest cells [32,33]. TNC is expressed in a disperse fashion and its remarkable features contribute to the development of boundary correlation with functional subdivision of neuroanatomy. Therefore, TNC is correlated with the process of cell migration and tissue remodeling [34]. At adult stage, TNC is absent from most regions of the normal brain and only persists in areas that permit continuous neuronal regeneration, such as stem cell niches of the subventricular zone and olfactory system [35,36]. Therefore, TNC should have a little influence on the transportation in ECS.

In contrast to TNC, TNR is another member of the Tenascin family that presents widespread expression throughout the caudate nucleus and thalamus. In the mature brain, TNR can interact with hyaluronan and chondroitin sulfate proteoglycans (Aggrecan, Neurocan, and Brevican) to form perineuronal nets. The mixture can protect neurons and stabilize synapses [37]. TNR located peri-axon can also interact with Versican and Phosphacan and participate in remyelination and axonal regeneration [38]. Some researchers found that the apparent diffusion coefficient increases in TNR knock-out rats and decreases in tumor tissues where the expression of TNR is extremely abundant [39]. However, the present study demonstrated that the effective diffusion coefficient increased in the thalamus where the expression of TNR was more abundant. Therefore, TNR should have a partly negative influence on tortuosity.

Versican is an enormous chondroitin sulfate proteoglycan located in the ECM around the myelinated fibers and is most often found around the Ranvier nodes. Versican is also a strong inhibitor of axonal growth and is believed to play a role in the decline of fundamental plasticity associated with myelination [38,40]. The expression of Versican is scattered in the caudate nucleus and is absent from the thalamus. Interestingly, the expression of Versican is also located at the boundary between the caudate nucleus and thalamus. Because the boundary seems to exert barrier functions hindering cross-regional transportation [41], Versican or its related tissues can restrict the diffusion of substances in the ECS.

The present study has several limitations. Firstly, more mathematical parameters, for example the maximal distribution volume and its time, need be calculated. Secondly, the physiological mechanism that results in the partitioned transportation needs to be evaluated. Thirdly, there are many factors influencing the transportation, and ECM is only one of them. Fourthly, in Eq. (1), volume fraction ( $\alpha$ ) can be varied slightly in different brain areas and may influence parameter values.

## Conclusions

We have recommended an innovative MRI tracer-based technique to globally visualize the dynamic transportation of tracer in the ECS of deep brain regions, and to quantify the transportation (effective diffusion coefficients) in the ECS and ECS nanostructure (tortuosity). Our study demonstrates partitioned transportation of substances located in the ECS of deep brain regions and different capabilities of transportation in the partition. The present study improves our understanding of the brain microenvironment, improves local drugs delivery, and highlights brain tissue engineering fields in the future, such as next-generation brain imaging and large-scale recording and modulation in the nerve center system.

## Acknowledgements:

The authors thank You Li and Hongbin Jin Laboratory at the Beijing University of Posts and Telecommunications for technical support.

## Conflicts of interest

None.



## References:

- Sykova E, Nicholson C: Diffusion in brain extracellular space. *Physiol Rev*, 2008; 88(4): 1277–340
- Lei Y, Han H, Yuan F et al: The brain interstitial system: Anatomy, modeling, *in vivo* measurement, and applications. *Progr Neurobiol*, 2016 [Epub ahead of print]
- Thorne RG, Nicholson C: *In vivo* diffusion analysis with quantum dots and dextrans predicts the width of brain extracellular space. *Proc Natl Acad Sci USA*, 2006; 103(14): 5567–72
- Le Bihan D, Johansen-Berg H: Diffusion MRI at 25: Exploring brain tissue structure and function. *Neuroimage*, 2012; 61(2): 324–41
- Kastellakis G, Cai DJ, Mednick SC et al: Synaptic clustering within dendrites: An emerging theory of memory formation. *Progr Neurobiol*, 2015; 126: 19–35
- He C, Chen F, Li B, Hu Z: Neurophysiology of HCN channels: From cellular functions to multiple regulations. *Progr Neurobiol*, 2014; 112: 1–23
- Xia J, Xie N, Feng Y et al: Brain susceptibility weighted imaging signal changes in acute hemorrhagic anemia: an experimental study using a rabbit model. *Med Sci Monit*, 2014; 20: 1291–97
- Li JL, Li CS, Fu JH et al: Evaluation of cranial and cervical arteries and brain tissue in transient ischemic attack patients with magnetic resonance angiography and diffusion-weighted imaging. *Med Sci Monit*, 2015; 21: 1726–31
- Grzesiakowska U, Tacikowska M: An assessment of the effectiveness of magnetic resonance imaging in delayed sequences after administration of Gd-DTPA contrast in the detection of metastatic lesions in the brain. *Med Sci Monit*, 2002; 8(1): MT21–24
- Mardor Y, Rahav O, Zauberman Y et al: Convection-enhanced drug delivery: Increased efficacy and magnetic resonance image monitoring. *Cancer Res*, 2005; 65(15): 6858–63
- Shoosmith CL, Buist R, Del Bigio MR: Magnetic resonance imaging study of extracellular fluid tracer movement in brains of immature rats with hydrocephalus. *Neurol Res*, 2000; 22(1): 111–16
- Han H, Li K, Yan J et al: An *in vivo* study with an MRI tracer method reveals the biophysical properties of interstitial fluid in the rat brain. *Sci China Life Sci*, 2012; 55(9): 782–87
- Han H, Shi C, Fu Y et al: A novel MRI tracer-based method for measuring water diffusion in the extracellular space of the rat brain. *IEEE J Biomed Health Inform*, 2014; 18(3): 978–83
- Caravan P, Ellison JJ, McMurry TJ, Lauffer RB: Gadolinium(III) chelates as MRI contrast agents: Structure, dynamics, and applications. *Chem Rev*, 1999; 99(9): 2293–52
- Xu F, Han H, Zhang H et al: Quantification of Gd-DTPA concentration in neuroimaging using T(1)3D MP-RAGE sequence at 3.0 T. *Magn Reson Imaging*, 2011; 29(6): 827–34
- Sykova E, Mazel T, Simonova Z: Diffusion constraints and neuron-glia interaction during aging. *Exp Gerontol*, 1998; 33(7–8): 837–51
- Lau LW, Cua R, Keough MB et al: Pathophysiology of the brain extracellular matrix: A new target for remyelination. *Nat Rev Neurosci*, 2013; 14(10): 722–29
- Crocker SJ, Pagenstecher A, Campbell IL: The TIMPs tango with MMPs and more in the central nervous system. *J Neurosci Res*, 2004; 75(1): 1–11
- Michel G, Tonon T, Scornet D et al: The cell wall polysaccharide metabolism of the brown alga *Ectocarpus siliculosus*. Insights into the evolution of extracellular matrix polysaccharides in Eukaryotes. *New Phytol*, 2010; 188(1): 82–97
- Wolak DJ, Thorne RG: Diffusion of macromolecules in the brain: Implications for drug delivery. *Mol Pharm*, 2013; 10(5): 1492–504
- Nicholson C, Phillips JM: Ion diffusion modified by tortuosity and volume fraction in the extracellular microenvironment of the rat cerebellum. *J Physiol*, 1981; 321: 225–57
- Abbott NJ: Evidence for bulk flow of brain interstitial fluid: Significance for physiology and pathology. *Neurochem Int*, 2004; 45(4): 545–52
- Xie Y, Ye LY, Zhang XB et al: [Establishment of an *in vitro* model of brain-blood barrier.] *Beijing Da Xue Xue Bao*, 2004; 36(4): 435–38 [in Chinese]
- Liu B, Bai X, Zhou F et al: Mutual information based three-dimensional registration of rat brain magnetic resonance imaging time-series \*. *Computers & Electrical Engineering*, 2013; 39(5): 1473–84
- Shi C, Lei Y, Han H et al: Transportation in the interstitial space of the brain can be regulated by neuronal excitation. *Sci Rep*, 2015; 5: 17673
- Paxinos G, Watson C: The rat brain in stereotaxic coordinates: Hard cover edition: Academic Press, 2006
- Shen XH, Wang BZ: [Structural foundations of the releasing pattern and transport route for hormone granules of neurohypophysis.] *Chinese Journal of Clinical Rehabilitation*, 2005 [in Chinese]
- Xi G, Robinson E, Mania-Farnell B et al: Convection-enhanced delivery of nanodiamond drug delivery platforms for intracranial tumor treatment. *Nanomedicine*, 2014; 10(2): 381–91
- Barua NU, Miners JS, Bienemann AS et al: Convection-enhanced delivery of neprilysin: A novel amyloid-beta-degrading therapeutic strategy. *J Alzheimers Dis*, 2012; 32(1): 43–56
- Anderson RC, Kennedy B, Yanes CL et al: Convection-enhanced delivery of topotecan into diffuse intrinsic brainstem tumors in children. *J Neurosurg Pediatr*, 2013; 11(3): 289–95
- Han H, Xia Z, Chen H et al: Simple diffusion delivery via brain interstitial route for the treatment of cerebral ischemia. *Sci China Life Sci*, 2011; 54(3): 235–39
- Tucker RP, McKay SE: The expression of tenascin by neural crest cells and glia. *Development*, 1991; 112(4): 1031–39
- Kawano H, Ohyama K, Kawamura K, Nagatsu I: Migration of dopaminergic neurons in the embryonic mesencephalon of mice. *Brain Res Dev Brain Res*, 1995; 86(1–2): 101–13
- Joester A, Faissner A: The structure and function of tenascins in the nervous system. *Matrix Biol*, 2001; 20(1): 13–22
- Gonzalez ML, Silver J: Axon-glia interactions regulate ECM patterning in the postnatal rat olfactory bulb. *J Neurosci*, 1994; 14(10): 6121–31
- Chiquet-Ehrismann R, Orend G, Chiquet M et al: Tenascins in stem cell niches. *Matrix Biol*, 2014; 37: 112–23
- Chiquet-Ehrismann R, Chiquet M: Tenascins: Regulation and putative functions during pathological stress. *J Pathol*, 2003; 200(4): 488–99
- Dours-Zimmermann MT, Maurer K, Rauch U et al: Versican V2 assembles the extracellular matrix surrounding the nodes of Ranvier in the CNS. *J Neurosci*, 2009; 29(24): 7731–42
- Zamecnik J, Vargova L, Homola A et al: Extracellular matrix glycoproteins and diffusion barriers in human astrocytic tumours. *Neuropathol Appl Neurobiol*, 2004; 30(4): 338–50
- Morawski M, Bruckner MK, Riederer P et al: Perineuronal nets potentially protect against oxidative stress. *Exp Neurol*, 2004; 188(2): 309–15
- Zuo L, Li K, Han H: Comparative analysis by magnetic resonance imaging of extracellular space diffusion and interstitial fluid flow in the rat striatum and thalamus. *Applied Magnetic Resonance*, 2015; 46(6): 623–32